

# Production and decays of the light pseudoscalar boson $\eta$ at the LHC

## in the simplest little Higgs model

Kingman Cheung<sup>1,2</sup>, Jeonghyeon Song<sup>3</sup>, Poyan Tseng<sup>1</sup>, Qi-Shu Yan<sup>1,2</sup>

<sup>1</sup> *Department of Physics, National Tsing Hua University, Hsinchu, Taiwan*

<sup>2</sup> *Physics Division, National Center for Theoretical Sciences, Hsinchu, Taiwan*

<sup>3</sup> *Department of Physics, Konkuk University, Seoul 143-701, Korea*

(Dated: June 21, 2024)

### Abstract

In many extensions of the standard model, the Higgs sector often contains an additional pseudoscalar boson. A good example is the SU(3) simplest little Higgs model, which accommodates a light pseudoscalar boson  $\eta$  with quite different characteristics from those in other multi-Higgs-doublet models. We study various phenomenological signatures of the  $\eta$  at the LHC. In particular, we calculate in details both production and decays in the Drell-Yan type channel  $q\bar{q} \rightarrow Z/Z' \rightarrow h\eta$ , and in the associated production with a  $t\bar{t}$  pair,  $gg(q\bar{q}) \rightarrow t\bar{t}\eta$ . We emphasize the  $\tau^+\tau^-$  decay mode of the  $\eta$  boson when its mass is below the  $b\bar{b}$  threshold. We show that  $t\bar{t}\eta$  production is in fact large enough to give a sizable number of events while suppressing the backgrounds. We also comment on the direct gluon fusion process and the indirect decay from the heavy  $T$  quark ( $T \rightarrow t\eta$ ).

PACS numbers:

## I. INTRODUCTION

One of the primary goals of the CERN Large Hadron Collider (LHC) is to understand the electroweak symmetry breaking, which is vital in explaining the origin of the fermion and gauge boson masses. In the standard model (SM), one single Higgs doublet is introduced to trigger the electroweak symmetry breaking, of which the by-product is a scalar boson known as the Higgs boson. Although the SM does not predict the mass of the Higgs boson ( $m_H$ ), we have direct, indirect, and theoretical bounds on  $m_H$ . The most up-to-date search has placed a lower bound of 114.4 GeV [1] on  $m_H$ . The precision measurements from LEP and SLD collaborations have placed an upper bound on  $m_H < 160$  GeV (at one-sided 95% C.L.) [2], which is much lighter than the theoretical one (the so-called triviality bound) of about 1 TeV. The consensus is that the Higgs boson is rather light.

The SM by itself cannot provide any theoretical framework to guarantee the lightness of the Higgs boson. Very often small masses are protected by some symmetries, *e.g.*, the chiral symmetry to protect fermion masses and the gauge symmetry to protect gauge boson masses. There are no such symmetries in the SM to protect the scalar boson masses. A recent class of models, dubbed the little Higgs models, has been developed based on the idea that the lightness of the Higgs boson is attributed to its being a pseudo Nambu-Goldstone boson (pNGB) [3]. Armed by the collective symmetry breaking idea, little Higgs models can explain the little hierarchy problem. The Higgs boson mass is radiatively generated with quadratic divergence emerging at two loop level: The Higgs boson mass around 100 GeV and the 10 TeV cut-off are possible without fine-tuning. The one-loop level quadratic divergences from the SM gauge boson and top-quark loops are canceled by those from new heavy gauge boson and heavy  $T$ -quark loops, respectively. According to the global symmetry breaking pattern little Higgs models can be classified into two categories: (i) the *product group* models where the diagonal breaking of two (or more) gauge groups leads to the SM gauge group, and (ii) the *simple group* models where a single larger gauge group is broken into the SM gauge group. The most studied *product group* model is the littlest Higgs model [4] while that for the *simple group* model is the simplest little Higgs model [5]. In this work, we focus on the simplest little Higgs (SLH) model, which generates the least fine tuning in explaining the low Higgs mass [6].

A special feature of the simplest little Higgs model is the presence of a light pseudoscalar

boson, denoted by  $\eta$ . The model is based on  $[\text{SU}(3) \times \text{U}(1)_X]^2$  global symmetry with its diagonal subgroup  $\text{SU}(3) \times \text{U}(1)_X$  gauged. The vacuum expectation values (VEV) of two  $\text{SU}(3)$ -triplet scalar fields,  $\langle \Phi_{1,2} \rangle = (0, 0, f_{1,2})^T$ , spontaneously break both the global symmetry and the gauge symmetry. Uneaten pNGB's consist of a  $\text{SU}(2)_L$  doublet  $h$  and a pseudoscalar  $\eta$ . In Ref. [7] it was pointed out that the  $\eta$  boson in the original model is massless, which is problematic for  $\eta$  production in rare  $K$  and  $B$  decays,  $B$ - $\bar{B}$  mixing, and  $\Upsilon \rightarrow \eta\gamma$ , as well as for the cosmological axion limit. One of the simplest remedies was suggested by introducing a  $-\mu^2(\Phi_1^\dagger\Phi_2 + h.c.)$  term into the scalar potential by hand [5, 8, 9]. This  $\mu$  term then determines the  $\eta$  mass. The mass of  $\eta$  is not theoretically constrained, but there exists an experimental constraint from non-observation in the decay  $\Upsilon \rightarrow \gamma + X_0$ . It excludes pseudoscalar bosons with mass below 5–7 GeV [10]. It has been also shown that a sizable portion of parameter space kinematically allows the decay  $h \rightarrow \eta\eta$ , which can relieve the constraint on the direct search bound on the Higgs boson mass [7, 11].

In this work, we focus on production and decays of a light  $\eta$  boson at the LHC. The decay pattern of  $\eta$  is quite similar to that of the SM Higgs boson. A few distinctive features are (i) the  $\eta$  does not decay into  $WW$  and  $ZZ$ , (ii)  $\eta$  has a rather large branching ratio into  $gg$ , and (iii) the dominant decay mode is  $\eta \rightarrow ZH$  if kinematically allowed. The largest production channel for  $\eta$  is gluon fusion, but the decay of  $\eta \rightarrow b\bar{b}, jj$  will be buried under QCD backgrounds while  $\eta \rightarrow \tau^+\tau^-$  will not likely stand out of the Drell-Yan background. The  $WW$  fusion does not contribute to  $\eta$  production. Associated production  $\eta$  with  $t\bar{t}$  pair and with the Higgs boson could be the most useful channels to search for the  $\eta$ .

The organization is as follows. In the next section, we describe briefly the simplest little Higgs model with the  $\mu$  term. We calculate the decays and production of the  $\eta$  boson in Sec. III and IV, respectively. We study the detection of the  $\eta$  boson in Sec. V and VI. We then conclude in Sec. VII.

## II. $\text{SU}(3)$ SIMPLEST GROUP MODEL WITH THE $\mu$ TERM

The  $\text{SU}(3)$  simplest little Higgs model is based on  $[\text{SU}(3) \times \text{U}(1)_X]^2$  global symmetry with its diagonal subgroup  $\text{SU}(3) \times \text{U}(1)_X$  gauged. The symmetry breaking of  $\text{SU}(3) \times \text{U}(1)_X \rightarrow \text{SU}(2)_L \times \text{U}(1)_Y$  is generated by aligned VEVs of two complex  $\text{SU}(3)$  triplet scalar fields,  $\Phi_1$  and  $\Phi_2$ . Out of the 10 degrees of freedom in  $\Phi_1$  and  $\Phi_2$ , five are eaten by the  $\text{SU}(3)$  symmetry

breaking. Remained five degrees of freedom in  $\Phi_{1,2}$  are parameterized as a nonlinear sigma model with

$$\Phi_1 = e^{it_\beta\Theta}\Phi_1^{(0)}, \quad \Phi_2 = e^{-i\Theta/t_\beta}\Phi_2^{(0)}, \quad (1)$$

where  $t_\beta \equiv \tan\beta$  and

$$\Theta = \frac{1}{f} \left[ \begin{pmatrix} 0 & 0 & h \\ 0 & 0 & h^\dagger \\ h^\dagger & 0 & 0 \end{pmatrix} + \frac{\eta}{\sqrt{2}} \begin{pmatrix} 1 & 0 & 0 \\ 0 & 1 & 0 \\ 0 & 0 & 1 \end{pmatrix} \right] \equiv \frac{h_0}{f} \widehat{\mathbb{H}} + \frac{\eta}{\sqrt{2}f} \mathbb{I}_3. \quad (2)$$

Radiatively generated VEV of the Higgs boson field  $h$  triggers the SM electroweak symmetry breaking (EWSB): The Higgs boson is defined by  $h = (v + h_0)/\sqrt{2}$ . Without resort to any expansion,  $\Phi_1$  and  $\Phi_2$  have the following closed form [7]:

$$\Phi_1 = f c_\beta e^{i\frac{t_\beta\eta}{\sqrt{2}f}} \begin{pmatrix} i \sin \frac{t_\beta h_0}{f} \\ 0 \\ \cos \frac{t_\beta h_0}{f} \end{pmatrix}, \quad \Phi_2 = f s_\beta e^{-i\frac{\eta}{\sqrt{2}t_\beta f}} \begin{pmatrix} -i \sin \frac{h_0}{t_\beta f} \\ 0 \\ \cos \frac{h_0}{t_\beta f} \end{pmatrix}. \quad (3)$$

Note that  $\eta$  in  $\Phi_{1,2}$  is only a phase factor. Explicit form of  $\partial_\mu\Phi_{1,2}$  are also useful for later discussions:

$$\begin{aligned} \partial_\mu\Phi_1 &= i s_\beta e^{i\frac{t_\beta\eta}{\sqrt{2}f}} \left\{ \frac{\partial\eta}{\sqrt{2}} + \partial h_0 \widehat{\mathbb{H}} \right\} \begin{pmatrix} i \sin \frac{t_\beta h_0}{f} \\ 0 \\ \cos \frac{t_\beta h_0}{f} \end{pmatrix}, \\ \partial_\mu\Phi_2 &= -i c_\beta e^{-i\frac{\eta}{\sqrt{2}t_\beta f}} \left\{ \frac{\partial\eta}{\sqrt{2}} + \partial h_0 \widehat{\mathbb{H}} \right\} \begin{pmatrix} -i \sin \frac{h_0}{t_\beta f} \\ 0 \\ \cos \frac{h_0}{t_\beta f} \end{pmatrix}. \end{aligned} \quad (4)$$

The covariant derivative term is

$$\mathcal{L}_\Phi = \sum_{j=1,2} \left| \left( \partial_\mu + i g A_\mu^a T^a - i \frac{g_x}{3} B_\mu^x \right) \Phi_j \right|^2 \equiv \sum_{j=1,2} |(\partial_\mu + i g \mathbb{G}_\mu) \Phi_j|^2, \quad (5)$$

where  $g_x = g t_W \sqrt{1 - t_W^2/3}$  and  $t_W$  is the tangent of the electroweak mixing angle. Detailed expressions for  $\mathbb{G}$  is referred to Ref. [12]. As  $\Phi_1$  and  $\Phi_2$  develop their VEVs, the 5 degrees of freedom appear as the longitudinal component of the heavy gauge bosons, including a  $Z'$  gauge boson and a complex SU(2) doublet ( $Y^0, X^-$ ), with masses

$$M_{Z'} = \sqrt{\frac{2}{3 - t_W^2}} g f, \quad M_{X^\pm} = M_Y = \frac{g f}{\sqrt{2}}. \quad (6)$$

For convenience we separate the Lagrangian in Eq. (5) into three terms:

$$\begin{aligned}\mathcal{L}_\Phi &= \sum_{j=1,2} |\partial_\mu \Phi_j|^2 + \sum_{j=1,2} \left[ -ig\Phi_j^\dagger \mathbb{G}^\mu \partial_\mu \Phi_j + H.c. \right] + g^2 \sum_{j=1,2} \Phi_j^\dagger \mathbb{G}^\mu \mathbb{G}_\mu \Phi_j \\ &\equiv \mathcal{L}_{kin} + \mathcal{L}_{int} + \mathcal{L}_{mass}.\end{aligned}\quad (7)$$

Using Eq. (3) it is easy to see that the first term is just the kinetic term of the Higgs boson and  $\eta$ :

$$\sum_{i=1,2} |\partial\Phi_i|^2 = \frac{(\partial\eta)^2}{2} + (\partial h_0)^2. \quad (8)$$

The last term  $\mathcal{L}_{mass}$  leads to the masses for the gauge bosons as well as the coupling of the Higgs boson with two gauge boson. Since  $\eta$  is only a phase factor in  $\Phi_{1,2}$ , the  $\eta$ -dependence in  $\mathcal{L}_{mass}$  disappears. From Eqs. (3) and (4), the second term  $\mathcal{L}_{int}$  leads to only the  $\eta$ - $H$ - $Z$ ,  $\eta$ - $H$ - $Z'$ , and  $\eta$ - $H$ - $\Im m(Y^0)$  couplings:

$$\begin{aligned}\mathcal{L}_{int} &= \sqrt{2} \left( t_\beta - \frac{1}{t_\beta} \right) \frac{m_Z}{f} (H\partial_\mu \eta - \eta\partial_\mu H) [Z^\mu - f_{Z'} Z'^\mu] \\ &\quad + \sqrt{2} g (H\partial_\mu \eta - \eta\partial_\mu H) \Im m(Y^{0\mu}),\end{aligned}\quad (9)$$

where  $f_{Z'} = c_W(1 - t_W^2)/\sqrt{3 - t_W^2} \approx 0.682$ .

The fermion sector in this model should be extended since the gauged SU(3) symmetry promotes the SM fermions into SU(3) triplets. The Yukawa interaction of the third generation quarks is determined by the little Higgs mechanism which cancels the largest contribution of the top quark to the radiative Higgs mass  $\delta m_H$ . However negligible contributions to  $\delta m_H$  of the first two generation quarks and all generation leptons leave some ambiguity in fermion embedding. In the literature, two kinds of fermion embedding have been discussed, the ‘‘universal’’ embedding [12], and the ‘‘anomaly-free’’ embedding [13]. In this paper we focus on the anomaly-free embedding case. The universal embedding case has almost the same Yukawa couplings of  $\eta$ , except that the first two generation heavy quarks are up-type while those in the anomaly-free embedding are down-type.

The quark Yukawa interactions for the third generation and for the first two generations are given by [12]

$$L_3 = i\lambda_1^t t_1^c \Phi_1^\dagger Q_3 + i\lambda_2^t t_2^c \Phi_2^\dagger Q_3 + i\frac{\lambda_d^m}{\Lambda} d_m^c \epsilon_{ijk} \Phi_1^i \Phi_2^j Q_3^k + H.c., \quad (10)$$

$$L_{1,2} = i\lambda_1^{d_n} d_{1n}^c Q_n^T \Phi_1 + i\lambda_2^{d_n} d_{2n}^c Q_n^T \Phi_2 + i\frac{\lambda_u^{mn}}{\Lambda} u_m^c \epsilon_{ijk} \Phi_1^{*i} \Phi_2^{*j} Q_n^k + H.c., \quad (11)$$

where  $n = 1, 2$ ;  $i, j, k = 1, 2, 3$  are SU(3) indices;  $Q_3 = \{t_L, b_L, iT_L\}$  and  $Q_n = \{d_{nL}, -u_{nL}, iD_{nL}\}$ ;  $d_m^c$  runs over  $(d^c, s^c, b^c, D^c, S^c)$ ;  $u_m^c$  runs over  $(u^c, c^c, t^c, T^c)$ .

The mass eigenstate  $(f^c, F^c)$  are the mixture of  $(f_1^c, f_2^c)$ , where  $f = t, s, c$  and  $F = T, S, C$ ,

$$\begin{pmatrix} t^c \\ T^c \end{pmatrix} = \begin{pmatrix} -\cos \theta_T & \sin \theta_T \\ \sin \theta_T & \cos \theta_T \end{pmatrix} \begin{pmatrix} t_1^c \\ t_2^c \end{pmatrix}, \quad \begin{pmatrix} d^c \\ D^c \end{pmatrix} = \begin{pmatrix} \cos \theta_{D,S} & \sin \theta_{D,S} \\ \sin \theta_{D,S} & -\cos \theta_{D,S} \end{pmatrix} \begin{pmatrix} d_1^c \\ d_2^c \end{pmatrix}, \quad (12)$$

where the  $s$  quark sector is the same as the  $d$  quark sector. The mixing angles are

$$\sin \theta_F = \frac{\lambda_1^f c_\beta}{\sqrt{(\lambda_1^f c_\beta)^2 + (\lambda_2^f s_\beta)^2}}, \quad \cos \theta_F = \frac{\lambda_2^f s_\beta}{\sqrt{(\lambda_1^f c_\beta)^2 + (\lambda_2^f s_\beta)^2}}, \quad (13)$$

where  $c_\beta = \cos \beta$  and  $s_\beta = \sin \beta$ .

The heavy quark masses  $(M_T, M_S, M_D)$  and the SM quark masses are

$$M_Q = \sqrt{(\lambda_1^q c_\beta)^2 + (\lambda_2^q s_\beta)^2} f, \quad m_q = \frac{\lambda_1^q \lambda_2^q}{\sqrt{2}} \frac{f}{M_Q} v, \quad \text{for } q = t, s, d, \quad Q = T, S, D, \quad (14)$$

Small masses of  $m_d$  and  $m_s$  are satisfied simply by the condition  $\lambda_1^{s,d} \ll \lambda_2^{s,d}$ , which implies

$$\theta_{D,S} \simeq 0. \quad (15)$$

Accepting this simplification, this model has the following five parameters:

$$f, m_\eta, t_\beta, x_\lambda (\equiv \lambda_1^t / \lambda_2^t), M_D, M_S. \quad (16)$$

In Ref. [7], it is shown that proper EWSB prefers rather large  $t_\beta$  around 10.

Focused on  $\eta$ , we put its Yukawa couplings as

$$\mathcal{L}_Y^\eta = -i \sum_f \frac{m_f}{v} y_f^\eta \eta \bar{f} \gamma_5 f + \frac{m_t}{v} (i\eta \bar{T} P_R t + H.c.), \quad (17)$$

where the index  $f$  includes all of the SM fermions and heavy fermions,  $m_f$  is the fermion mass,  $v$  is the Higgs VEV, and  $T$  is the heavy top partner. We ignore  $\eta$ - $D$ - $d$  and  $\eta$ - $S$ - $s$  couplings due to their small mixing angles in Eq.(15). The parameter  $y_f^\eta$  indicates the ratio of the  $\eta$  Yukawa coupling to the SM Higgs Yukawa coupling, given by

$$\begin{aligned} y_l^\eta &= y_{d,s}^\eta = y_b^\eta = -y_{u,c}^\eta = -y_t^\eta = \frac{\sqrt{2}v}{f} \cot 2\beta, \\ y_Q^\eta &= -\frac{v}{f} [\cos 2\beta + \cos 2\theta_Q] \csc 2\beta, \quad \text{for } Q = D, S, T \end{aligned} \quad (18)$$

where  $l = e, \mu, \tau$ .

### III. $\eta$ DECAY

For  $m_\eta < m_Z + m_H$ , the  $\eta$  decays dominantly into a pair of SM fermions that is kinematically allowed. The decay rate of  $\eta \rightarrow f\bar{f}$  is

$$\Gamma(\eta \rightarrow f\bar{f}) = \frac{N_C}{8\pi} \left( \frac{m_f y_f^\eta}{v} \right)^2 m_\eta \lambda_\eta^{1/2}, \quad (19)$$

where  $\lambda_\eta = 1 - 4m_f^2/m_\eta^2$ , and  $N_C$  is the color factor of the fermion  $f$ . Since  $\Gamma(H \rightarrow f\bar{f})$  has a factor of  $\lambda_H^{3/2}$ , a pseudoscalar boson  $\eta$  with mass just above twice of a fermion mass has larger decay rate. Since the decay rate is proportional to the fermion mass,  $\eta$  boson with  $m_\eta < 2m_t$  mainly decays into a  $b\bar{b}$  pair. In the following calculation of decay widths, we use the running mass of the quarks evaluated at the scale  $m_\eta$  to calculate the Yukawa coupling, but not in the phase space factor. This is why the partial width into  $c\bar{c}$  is smaller than that into  $\tau^+\tau^-$ .

As in the Higgs boson case, the radiative decay rates of  $\eta$  into  $gg$  and  $\gamma\gamma$  are also important. Since  $\eta$  has no coupling with the *charged* gauge bosons, the partial decay widths into  $\gamma\gamma$  and  $gg$  are, respectively,

$$\Gamma(\eta \rightarrow gg) = \frac{\alpha_s^2 m_\phi^3}{32\pi^3 v^2} \left| \sum_f \frac{1}{2} y_f^\eta F_{1/2}^\eta(\tau_f) \right|^2, \quad (20)$$

$$\Gamma(\eta \rightarrow \gamma\gamma) = \frac{\alpha^2 m_\phi^3}{256\pi^3 v^2} \left| \sum_f y_f^\eta N_C^f Q_f^2 F_{1/2}^\eta(\tau_f) \right|^2, \quad (21)$$

where  $\tau_f = 4m_f^2/m_\eta^2$ ,  $N_C^f$  and  $Q_f$  are, respectively, the color factor and the electric charge of the fermion running in the loop. The dimensionless loop factor  $F_{1/2}^\eta(\tau)$  is

$$F_{1/2}^\eta(\tau) = -2\tau f(\tau), \quad (22)$$

with

$$f(\tau) = \begin{cases} [\sin^{-1}(1/\sqrt{\tau})]^2, & \tau \geq 1, \\ -\frac{1}{4}[\ln(\eta_+/\eta_-) - i\pi]^2, & \tau < 1, \end{cases} \quad \eta_\pm = 1 \pm \sqrt{1-\tau}. \quad (23)$$

For  $m_\eta$  above the  $b\bar{b}$  threshold the dominant decay mode is into the  $b\bar{b}$  pair. However, due to huge QCD background it is very difficult to identify the  $\eta$  boson in this mode, unless it is produced associated with some leptonic final states. The same difficulty is expected for  $\eta \rightarrow gg$ . On the other hand, the decay mode into  $\tau^+\tau^-$  could be useful, especially for

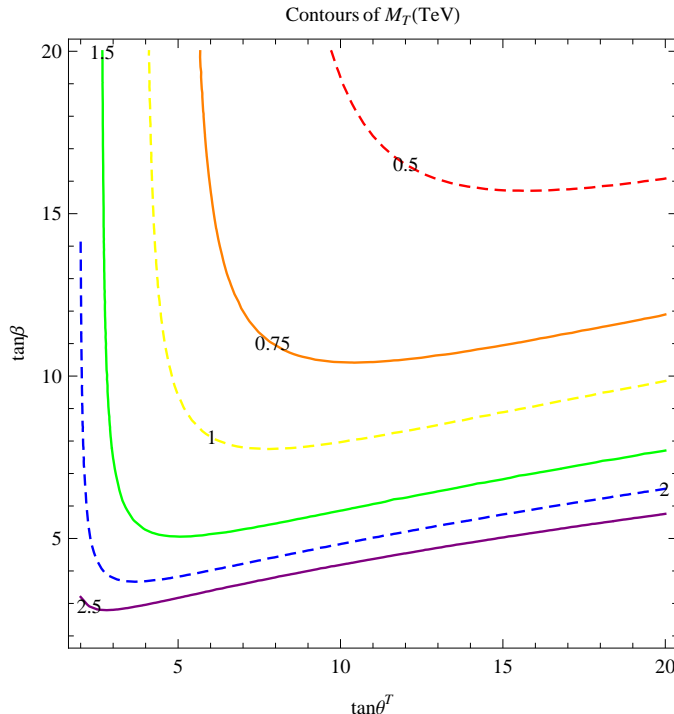


FIG. 1: The dependence of  $M_T$  (in unit of TeV) on  $\tan \beta \equiv t_\beta$  and  $\tan \theta_T$ . We have set  $f = 4$  TeV.

$2m_\tau < m_\eta < 2m_b$ . In this mass range, about 50% branching ratio is possible for  $\eta \rightarrow \tau^+\tau^-$ . We shall concentrate on this mode in Sec. V.

In Fig. 1, we show the dependence of  $M_T$  on  $t_\beta$  and  $\tan \theta_T$ . We have set  $m_D = 1.53$  TeV and  $m_S = 1.76$  TeV. Since proper EWSB can be achieved by large  $t_\beta$  around 10, the heavy top mass is somewhat sensitive to  $\tan \theta_T$ : For  $\tan \theta_T > 5$ ,  $M_T$  is relatively light below 1 TeV; for  $\tan \theta_T < 5$ ,  $M_T$  becomes heavier above 1 TeV.

In Fig. 2 (a)–(c), we show the contours of  $\text{Br}(\eta \rightarrow b\bar{b})$ ,  $\text{Br}(\eta \rightarrow gg)$ , and  $\text{Br}(\eta \rightarrow \gamma\gamma)$ , respectively, in  $(m_\eta, \tan \beta \equiv t_\beta)$  plane. The presented value for  $\eta \rightarrow b\bar{b}$  and  $\eta \rightarrow gg$  is in unit of  $10^{-2}$ , while that for  $\eta \rightarrow \gamma\gamma$  is in unit of  $10^{-4}$ . We vary  $m_\eta \in [20, 120]$  GeV, and  $t_\beta \in [2, 20]$ . The branching ratios are quite sensitive to  $m_\eta$ , but relatively insensitive to  $t_\beta$ . As in Fig. 1, we used  $m_T > 500$  GeV,  $m_D = 1.53$  TeV and  $m_S = 1.76$  TeV.

In Fig. 3, we show the branching ratios for the dominant decay modes of  $\eta$ . For  $m_\eta < 2m_c$   $\text{Br}(\eta \rightarrow gg)$  is the largest, whereas in the range  $2m_c < m_\eta < 2m_\tau$   $\text{Br}(\eta \rightarrow c\bar{c})$  is the largest. For  $2m_\tau < m_\eta < 2m_b$ , the largest is  $\text{Br}(\eta \rightarrow \tau^+\tau^-)$ , followed by  $\text{Br}(\eta \rightarrow c\bar{c})$ . When  $2m_b < m_\eta < 120$  GeV,  $\text{Br}(\eta \rightarrow b\bar{b})$  becomes dominant. As  $m_\eta$  further increases, however,  $\text{Br}(\eta \rightarrow gg)$  takes over. This is due to the enhancement from the contributions of heavy  $T$ ,

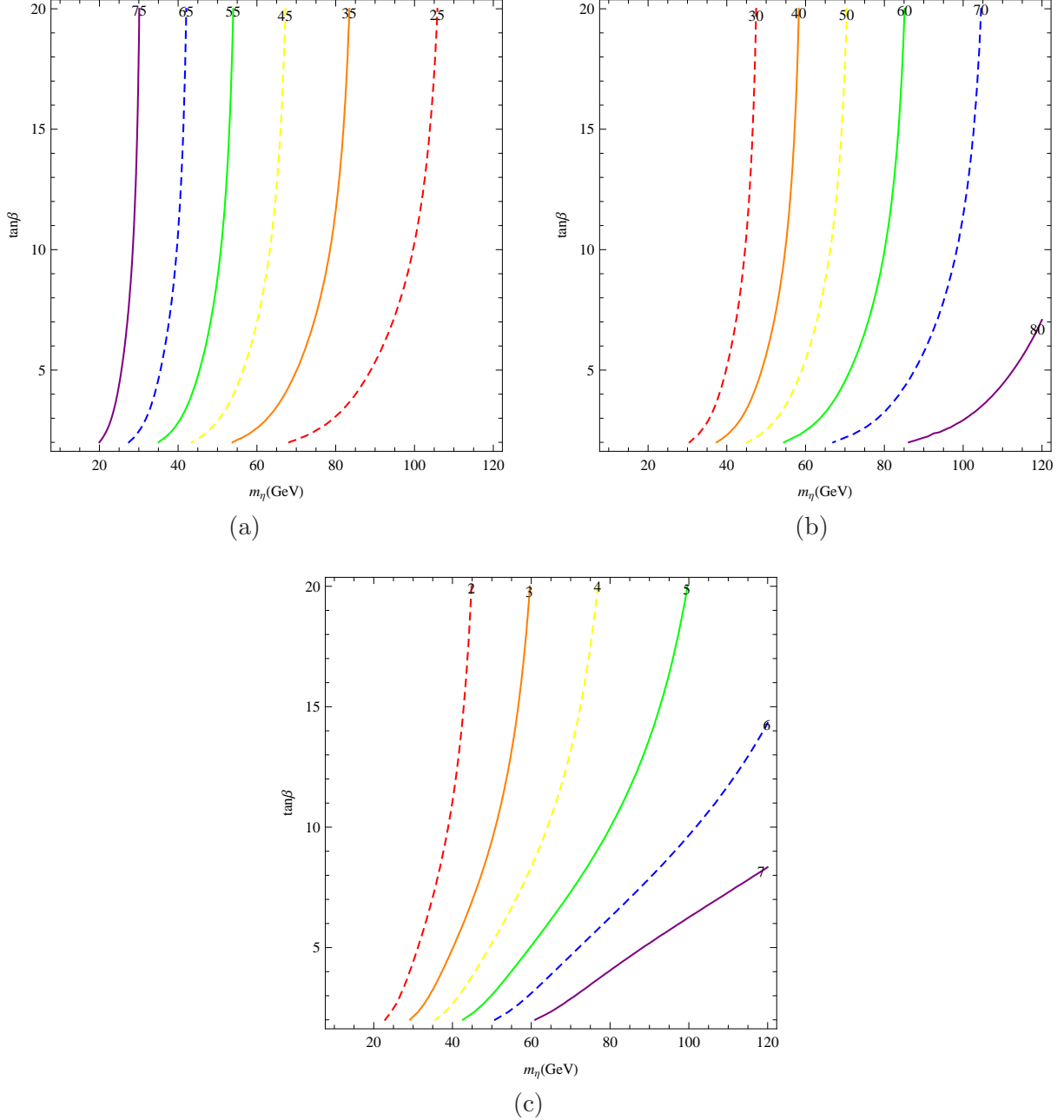


FIG. 2: Contour plots of  $\text{Br}(\eta \rightarrow b\bar{b}) \times 10^2$  in (a),  $\text{Br}(\eta \rightarrow gg) \times 10^2$  in (b), and  $\text{Br}(\eta \rightarrow \gamma\gamma) \times 10^4$  in (c) on  $m_\eta$  and  $\tan \beta \equiv t_\beta$  plane. The parameter  $f$  is fixed at 4 TeV.

$D$  and  $S$ , which are non-decoupled in the triangle loops. Such an enhancement is helpful for  $\eta$  production at the LHC via gluon fusion. On the other hand,  $\text{Br}(\eta \rightarrow \gamma\gamma)$  is only at the level  $10^{-4}$  in most of the parameter space. This is due to the absence of the  $\eta$ -coupling with charged gauge bosons.

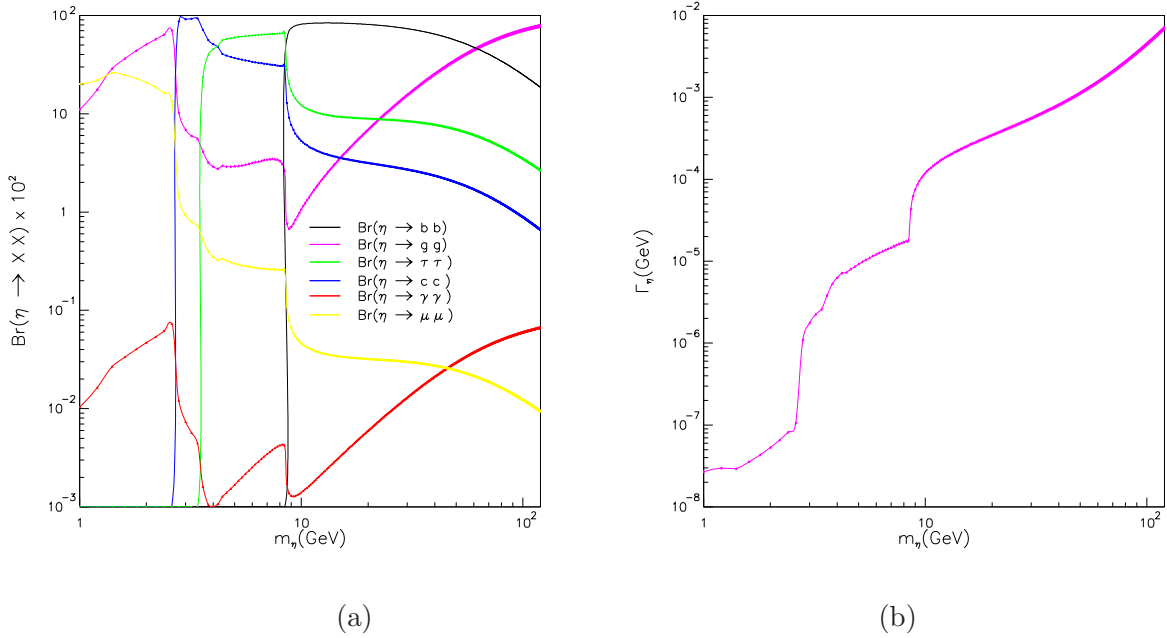


FIG. 3: (a) Branching ratios and (b) total decay width of  $\eta$  for  $1 \text{ GeV} < m_\eta < 120 \text{ GeV}$ . We fix  $t_\beta = 20$  and  $f = 4 \text{ TeV}$ .

#### IV. $\eta$ PRODUCTION AT THE LHC

Main production channels for  $\eta$  at the LHC are, in the order of the size of cross sections,

1. gluon fusion:  $gg \rightarrow \eta$ ;
2.  $b\bar{b}$  fusion:  $b\bar{b} \rightarrow \eta$ ;
3. associated production with  $H$ :  $q\bar{q} \rightarrow Z, Z', \Im m(Y^0) \rightarrow H\eta$ ;
4. associated production with  $t\bar{t}$ :  $gg, q\bar{q} \rightarrow t\bar{t}\eta$ ; and
5. decay from  $T$ :  $T \rightarrow t\eta$  and  $\bar{T} \rightarrow \bar{t}\eta$ .

The resulting cross sections are to be compared in subsection F.

### A. Gluon fusion

For gluon fusion the cross section at  $pp$  hadron collider with the c.m. energy  $s$  ( $\sqrt{s} = 14$  TeV for the LHC) is

$$\sigma(gg \rightarrow \eta) = \int_{\tau_\eta}^1 \frac{dx}{x} f_{g/p}(x) f_{g/p}\left(\frac{\tau_\eta}{x}\right) \tau_\eta \sigma_0(gg \rightarrow \eta), \quad (24)$$

where  $\tau_\eta = m_\eta^2/s$ ,  $f_{g/p}$  is the parton distribution function of a gluon inside a proton, and

$$\sigma_0(gg \rightarrow \eta) = \frac{\pi^2}{8m_\eta^3} \Gamma(\eta \rightarrow gg). \quad (25)$$

### B. $b\bar{b}$ fusion

For the  $b\bar{b}$  fusion the cross section is

$$\begin{aligned} \sigma(b\bar{b} \rightarrow \eta) &= \int_{\tau_\eta}^1 \frac{dx}{x} \left[ f_{b/p}(x) f_{\bar{b}/p}\left(\frac{\tau_\eta}{x}\right) + f_{\bar{b}/p}(x) f_{b/p}\left(\frac{\tau_\eta}{x}\right) \right] \tau_\eta \sigma_0(b\bar{b} \rightarrow \eta) \\ &= 2 \int_{\tau_\eta}^1 \frac{dx}{x} f_{b/p}(x) f_{\bar{b}/p}\left(\frac{\tau_\eta}{x}\right) \tau_\eta \sigma_0(b\bar{b} \rightarrow \eta), \end{aligned} \quad (26)$$

where

$$\sigma_0(b\bar{b} \rightarrow \eta) = \frac{4\pi^2}{9m_\eta^3} \Gamma(\eta \rightarrow b\bar{b}). \quad (27)$$

### C. $H\eta$ associated production

The process of  $q\bar{q} \rightarrow \eta H$  is mediated by  $Z$ ,  $Z'$ , and  $\Im m(Y^0)$  gauge bosons. Since the gauge coupling of  $Y^0$  with the SM fermion is suppressed by  $v/f$  and  $1/t_\beta$ , we ignore it in the following. The interaction Lagrangian is parameterized by

$$\mathcal{L} = -g_Z \sum_{i,q} \bar{q} \gamma_\mu [g_{iR}^q P_R + g_{iL}^q P_L] Z_i^\mu + \sum_{i,q} c_i [H \partial_\mu \eta - \eta \partial_\mu H] Z_i^\mu, \quad (28)$$

where  $g_Z = g/c_W$ ,  $i = 1, 2$ ,  $Z_{1,2} = Z, Z'$ , and

$$g_{1R}^q = -x_W Q_q, \quad g_{1L}^q = (T_3^q)_L - x_W Q_q, \quad (29)$$

$$g_{2R}^q = \frac{Q_q x_W}{\sqrt{3 - 4x_W}}, \quad g_{2L}^q = \frac{1}{\sqrt{3 - 4x_W}} \left( -\frac{1}{2} + \frac{2}{3} x_W \right), \quad q = u, d, c, s,$$

$$g_{2R}^b = -\frac{1}{3} \frac{x_W}{\sqrt{3 - 4x_W}}, \quad g_{2L}^b = \frac{1}{\sqrt{3 - 4x_W}} \left( \frac{1}{2} - \frac{1}{3} x_W \right),$$

$$c_1 = \sqrt{2} \left( t_\beta - \frac{1}{t_\beta} \right) \frac{m_Z}{f}, \quad c_2 = -\sqrt{2} \left( t_\beta - \frac{1}{t_\beta} \right) \frac{m_Z}{f} f_{Z'}. \quad (30)$$

Here  $x_W = \sin^2 \theta_W$  and  $f_{Z'} = c_W(1 - t_W^2)/\sqrt{3 - t_W^2} \approx 0.682$ .

For the process of

$$q(p_1) + \bar{q}(p_2) \rightarrow \eta(k_1) + H(k_2), \quad (31)$$

the parton level differential cross section is

$$\frac{d\hat{\sigma}}{d\cos\theta^*}(q\bar{q}' \rightarrow \eta H) = \frac{\lambda^{1/2}(m_\eta^2/\hat{s}, m_H^2/\hat{s})}{36\pi\hat{s}} \frac{1}{3} (|\hat{g}_{qL}|^2 + |\hat{g}_{qR}|^2)(1 - \cos^2\theta^*), \quad (32)$$

where  $\theta^*$  is the scattering angle of  $\eta$  with respect to the incoming quark  $q$  in the parton c.m. frame,  $\hat{s} = (p_1 + p_2)^2$ , and  $\lambda(a, b) = 1 + a^2 + b^2 - 2a - 2b - 2ab$ . The effective couplings  $\hat{g}_{qL, qR}$  are

$$\hat{g}_{qX} = \sum_{i=1,2} \frac{\hat{s}}{\hat{s} - m_i^2 + im_i\Gamma_i} g_Z c_i g_{iX}^q, \quad \text{for } X = R, L. \quad (33)$$

The cross section of  $pp$  collision is then

$$\begin{aligned} \sigma(pp \rightarrow \eta H) = & \int dx_A dx_B \left[ \{f_{u/p}(x_A) f_{\bar{u}/p}(x_B) + f_{c/p}(x_A) f_{\bar{c}/p}(x_B)\} \hat{\sigma}(u\bar{u} \rightarrow \eta H) \right. \\ & + \{f_{d/p}(x_A) f_{\bar{d}/p}(x_B) + f_{s/p}(x_A) f_{\bar{s}/p}(x_B) + f_{b/p}(x_A) f_{\bar{b}/p}(x_B)\} \hat{\sigma}(d\bar{d} \rightarrow \eta H) \\ & \left. + (A \leftrightarrow B) \right] \end{aligned} \quad (34)$$

where  $f_{a/A}$  is the parton density of  $a$  inside the hadron  $A$ .

#### D. $t\bar{t}\eta$ associated production

There are two contributing subprocesses:

$$q\bar{q} \rightarrow t\bar{t}\eta, \quad gg \rightarrow t\bar{t}\eta.$$

The latter dominates at the LHC energy because of large gluon luminosity. We write down the helicity amplitudes in the appendix, and use FORM to evaluate the square of the amplitudes.

#### E. In the $T$ decay $T \rightarrow t\eta$

A pair of  $T\bar{T}$  is produced by QCD interactions, similar to a top-quark pair. When the  $T$  is heavy enough, single- $T$  production is kinematically advantageous [14]. In little Higgs

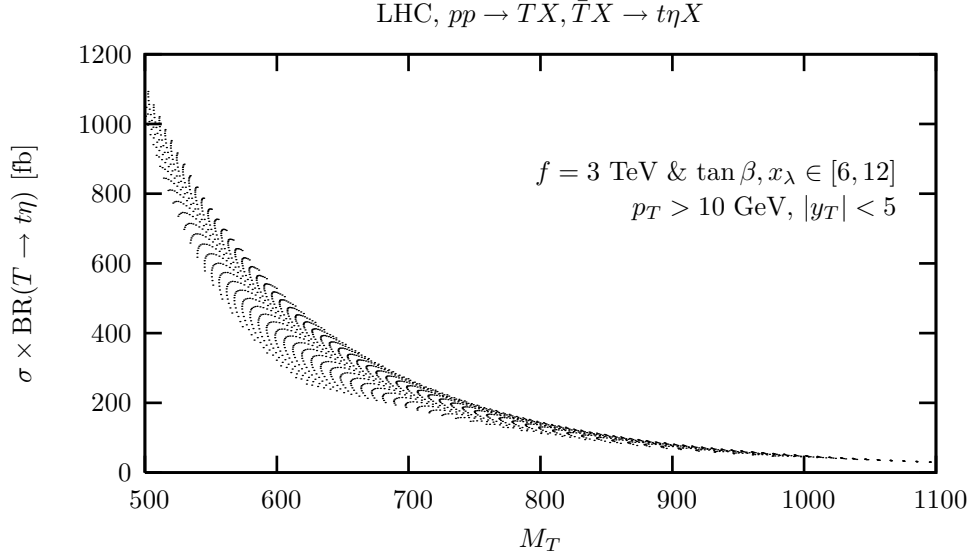


FIG. 4: Sum of cross sections of  $pp \rightarrow TX$  and  $pp \rightarrow \bar{T}X'$ , multiplied by the branching ratio of  $T \rightarrow t\eta$  in units of fb. We fix  $f = 3$  TeV, while varying  $t_\beta \in [6, 12]$  and  $x_\lambda \in [6, 12]$ .

models, the heavy  $T$  quark decays dominantly into  $tH$ ,  $tZ$ , and  $bW$  [12]. When neglecting final-state masses over  $M_T$ , the partial decay rates are

$$\Gamma(T \rightarrow tH) = \Gamma(T \rightarrow tZ) = \frac{1}{2} \Gamma(T \rightarrow bW) = \frac{\lambda_T^2}{32\pi} M_T, \quad (35)$$

where

$$\lambda_T = \frac{t_\beta}{t_\beta^2 + 1} \left( x_\lambda - \frac{1}{x_\lambda} \right) \frac{m_t}{v}. \quad (36)$$

Here  $x_\lambda = \lambda_1^t / \lambda_2^t$ . If these are the only decay modes of  $T$ , the branching ratios of  $T$  would show simple relation of  $\text{Br}(T \rightarrow tH) : \text{Br}(T \rightarrow tZ) : \text{Br}(T \rightarrow bW) = 1 : 1 : 2$ . However the SLH model allows another important decay mode of  $T \rightarrow t\eta$ . Its partial decay rate is

$$\Gamma(T \rightarrow t\eta) = \frac{1}{32\pi} \frac{m_t^2}{v^2} M_T. \quad (37)$$

Since EWSB prefers large  $t_\beta$  so that  $\lambda_T$  is suppressed if  $x_\lambda$  is not as large as  $t_\beta$ , this decay mode can be important. For example, two benchmark points in Ref.[11] have sizable decay rate of  $T \rightarrow \eta t$ :  $\text{Br}(T \rightarrow \eta t) \approx 45\%$  in the SHL $\mu$ -A case and  $\text{Br}(T \rightarrow \eta t) \approx 21\%$  in the SHL $\mu$ -B case.

In Fig.4, we show the production cross section of a single heavy top  $T$  at the LHC, multiplied by its branching ratio for  $T \rightarrow t\eta$ . We fix  $f = 3$  TeV and  $x_\lambda = 7, 12$ , and vary  $t_\beta$  and  $x_\lambda$  in the range between 6 and 12. We have included the single- $T$  production as

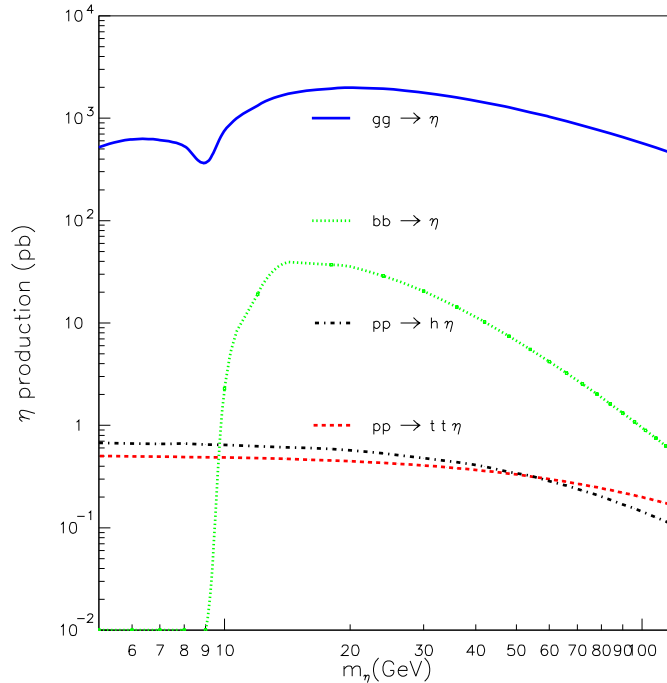


FIG. 5: Various production cross sections for  $\eta$  at the LHC in the mass range  $5 \text{ GeV} < m_\eta < 120 \text{ GeV}$ . We fix  $\tan \beta \equiv t_\beta = 20$  and  $f = 4 \text{ TeV}$ .

well as the single- $\bar{T}$  production. As stressed in Ref.[14], the non-negligible  $2 \rightarrow 3$  process of  $qg \rightarrow T\bar{b}q'$  with its charge-conjugated production is also included. Only for very optimal case of  $M_T$  around 500 GeV, the  $\eta$  production from the  $T$  decay can reach 1 pb.

## F. Comparisons

In Fig.5, we show the production cross sections against the mass of the  $\eta$  for various production channels at the LHC. The most dominant production channel is the gluon fusion, followed by the  $b\bar{b}$  fusion. In both channels, there is only  $\eta$  in the final state, which will decay into either a  $b\bar{b}$  pair or  $\tau^+\tau^-$  pair depending on  $m_\tau$ . Both modes suffer, respectively, from large QCD background and the Drell-Yan background. We do not consider these two production channels in the subsequent sections. In the associated production of  $h\eta$ , one has the addition  $h \rightarrow b\bar{b}$  decay to put the handle on. We will study this channel in detail in the next section. Another channel of interest is the  $t\bar{t}\eta$ . We will consider the signal-background

in Sec. VI. Finally, one should not ignore the  $\eta$ 's from the decay of the heavy  $T$ . As long as  $T$  is not too heavy such that its production rate is sizable, we expect enough  $\eta$ 's from  $T$  decays.

## V. THE SIGNAL AND BACKGROUND OF THE PROCESS $pp \rightarrow h\eta \rightarrow b\bar{b}\tau^-\tau^+$

In this section, we study the signal and backgrounds of the  $\eta$  production associated with the Higgs boson. To enhance the signal, we consider the following mass ranges of  $h$  and  $\eta$  where the subsequent decay of  $h \rightarrow b\bar{b}$  and  $\eta \rightarrow \tau^+\tau^-$  are important:

$$2m_\tau < m_\eta < 2m_b, \quad 114 \text{ GeV} < m_h < 2m_W. \quad (38)$$

Then  $pp \rightarrow h\eta$  production has the dominant decay mode of  $b\bar{b}\tau^+\tau^-$  without missing transverse energy. The kinematic cuts imposed on  $b$ 's and  $\tau$ 's are

$$p_T(j) > 15 \text{ GeV}, \quad p_T(\tau) > 10 \text{ GeV}, \quad |y_{j,l}| < 2.5, \quad \Delta R > 0.4. \quad (39)$$

The reconstruction efficiencies of  $b$  and  $\tau$  are taken as 0.5 and 0.4, respectively. The rejection rates of gluon and light quarks faking  $\tau$  are taken as 300, while the rejection rate of  $c$  quark faking  $\tau$  is taken as 20 [15]. To simulate the detector effects, we smear the energies of the jets and  $\tau$ 's with the following Gaussian resolutions

$$\frac{\Delta E_j}{E_j} = \frac{50\%}{\sqrt{E_j}} \oplus 3\%, \quad (40)$$

$$\frac{\Delta E_\tau}{E_\tau} = \frac{10\%}{\sqrt{E_\tau}} \oplus 0.7\%, \quad (41)$$

where  $E_{j,\tau}$  are measured in GeV. We also introduce the following invariant mass cuts on  $m_{b\bar{b}}$  and  $m_{\tau\tau}$  to suppress the backgrounds:

$$m_h - 10 \text{ GeV} < m_{b\bar{b}} < m_h + 10 \text{ GeV},$$

$$m_\eta - 2 \text{ GeV} < m_{\tau\tau} < m_\eta + 2 \text{ GeV}. \quad (42)$$

To further suppress the background from  $t\bar{t} \rightarrow b\bar{b}\tau^+\tau^- + \cancel{E}_T$ , we reject events with the missing transverse energy  $\cancel{E}_T > 50 \text{ GeV}$ , which is about the threshold of the missing transverse energy signature of CMS and ATLAS detectors. We observe that this cut can reduce the  $t\bar{t}$  background by 2/3. For Fig. 6, we present the Higgs mass and its branching ratio into  $b\bar{b}$

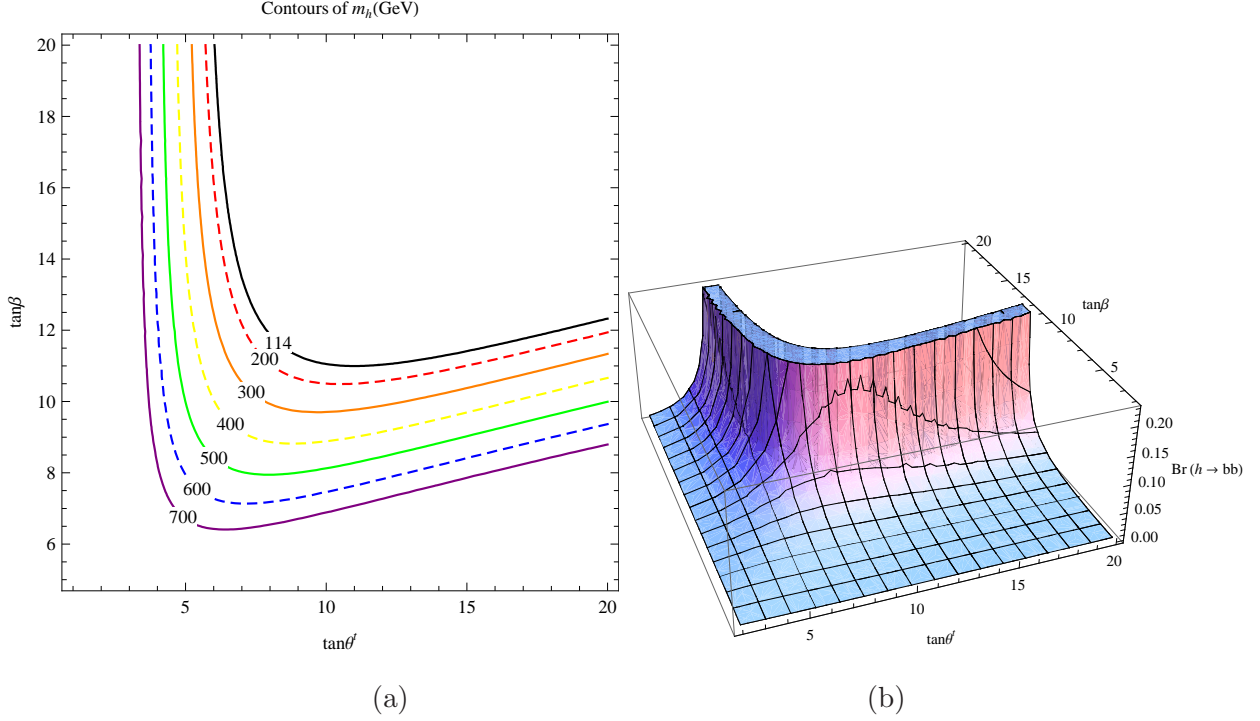


FIG. 6: (a) The mass of the Higgs boson in units of GeV and (b)  $\text{Br}(h \rightarrow b\bar{b})$  in the two-dimensional  $\tan \theta_T - t_\beta$  plane. We fix  $f = 4$  TeV.

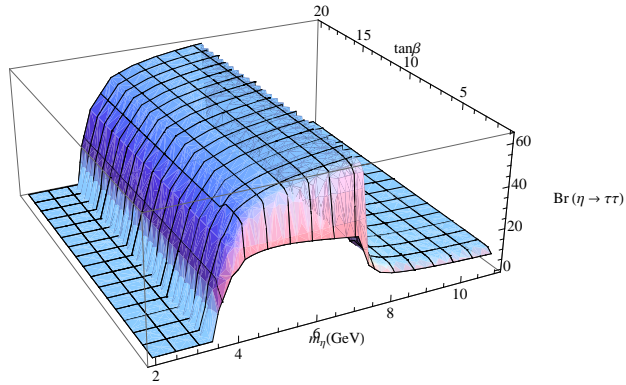


FIG. 7: The branching ratio  $\text{Br}(\eta \rightarrow \tau^+ \tau^-)$  in unit of  $10^{-2}$  for  $f = 4$  TeV.

in the plane of  $\tan \theta_T$  and  $t_\beta$  with fixed  $f = 4$  TeV. The branching ratio  $\text{Br}(\eta \rightarrow \tau^- \tau^+)$  is given in Fig. 7, which is almost insensitive to the value of  $t_\beta$ .

In order to simulate the signal, we select the following benchmark point:

$$f = 4 \text{ TeV}, \quad \tan \theta_T = 6.03, \quad t_\beta = 20, \quad m_\eta = 8 \text{ GeV}. \quad (43)$$

The relevant physics quantities corresponding to this benchmark point are  $\Gamma_\eta = 3.8 \times 10^{-5}$

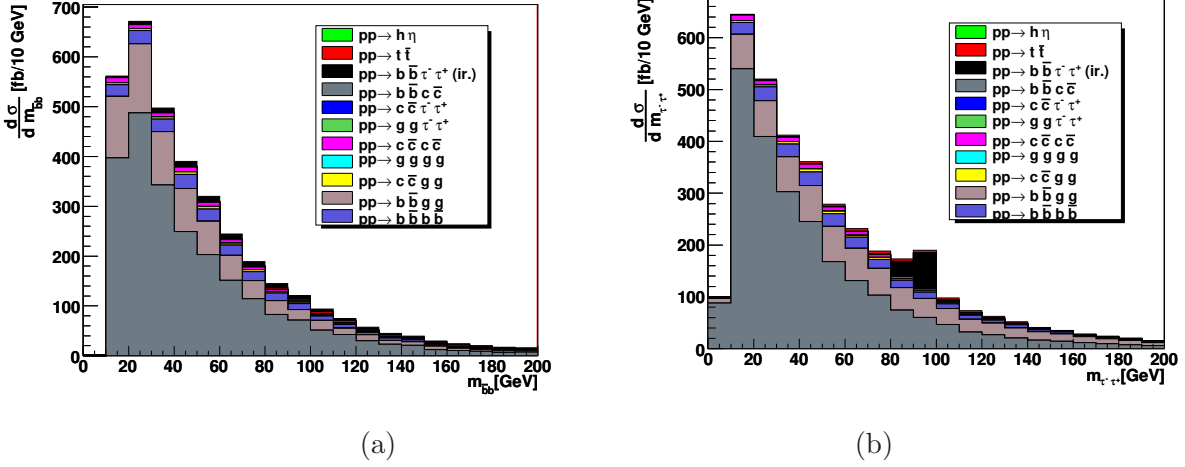


FIG. 8: The invariant mass distributions of (a)  $m_{b\bar{b}}$  and (b)  $m_{\tau\tau}$  for the signal and various backgrounds in  $pp \rightarrow h\eta \rightarrow b\bar{b}\tau^-\tau^+$  after imposing the selection cuts.

GeV,  $\text{Br}(\eta \rightarrow \tau^+\tau^-) = 38.5\%$ ,  $m_h = 115$  GeV,  $\Gamma_h = 6.6 \times 10^{-3}$  GeV,  $\text{Br}(h \rightarrow b\bar{b}) = 88.7\%$  and  $\text{Br}(h \rightarrow \eta\eta) = 0.43\%$ . The  $Z$ - $h$ - $\eta$  coupling in Eq. (9) is about 0.312 at the benchmark point. The small branching ratio of  $h \rightarrow \eta\eta$  is due to the small  $m_\eta$ . At this benchmark point, the  $Z'$  is quite heavy and does not appreciably contribute to  $pp \rightarrow h\eta$ .

We have several comments on the decay properties of  $h$  and  $\eta$  in the mass region  $2m_\tau < m_\eta < 2m_b$ .

1. The main decay channels of  $\eta$  are  $\eta \rightarrow \tau^+\tau^-$  and  $\eta \rightarrow c\bar{c}$ . The branching ratio of  $\eta \rightarrow \tau^+\tau^-$  is the largest due to the fact that QCD corrections to  $\text{Br}(\eta \rightarrow c\bar{c})$  encoded in the running mass  $m_c$  make it substantially smaller than that of  $\text{Br}(\eta \rightarrow \tau^+\tau^-)$ , even though the pole mass of charm quark is close to tau pole mass and this channel has a color factor of 3. In this mass region, the branching ratio  $\text{Br}(\eta \rightarrow \tau^+\tau^-)$  is not sensitive to the parameter  $t_\beta$ .
2. The mass of Higgs is not sensitive to the change of  $m_\eta$  due to the smallness of  $m_\eta$ .
3. The decay mode of  $h \rightarrow \eta\eta$  is small unlike the case in Refs. [7, 11], because here the mass of  $\eta$  is small and the decay rate is proportional to  $m_\eta^4$ .

In Fig.8, we show the signal and various backgrounds in both  $m_{b\bar{b}}$  and  $m_{\tau\tau}$  invariant mass distributions. It is clear that the signal is buried under the background and can hardly be seen. From these two plots, we can identify that the  $pp \rightarrow b\bar{b}c\bar{c}$  is the most dominant

Background processes	Cross Section (fb)
$b\bar{b}c\bar{c}$	1.87
$b\bar{b}g\bar{g}$	0.38
$c\bar{c}g\bar{g}$	0.06
$c\bar{c}c\bar{c}$	0.05
Signal processes	Cross Section (fb)
$b\bar{b}\tau^-\tau^+$	0.33

TABLE I: Background and signal cross sections in  $pp \rightarrow h\eta \rightarrow b\bar{b}\tau^+\tau^-$  after imposing all the cuts and tagging efficiencies.

background. In order to separate the signal of  $pp \rightarrow h\eta$  it is crucial to enhance the rejection factor for  $c$  quark faking  $\tau$ . The final signal and background rates are tabulated in Table I.

A few more comments on the signal are in order here.

1. The raw cross section of  $pp \rightarrow h\eta$  is around 1 pb. With the branching ratios of  $\text{Br}(h \rightarrow b\bar{b})$  and  $\text{Br}(\eta \rightarrow \tau^-\tau^+)$ , the signal is around 300 fb. After imposing the cuts on  $\Delta R(b, \bar{b})$ ,  $\Delta R(\tau^+, \tau^-)$ ,  $y_b$  and  $y_\tau$ , the signal is reduced to 90 fb. In addition, the  $p_T$  cuts on  $b$ 's and  $\tau$ 's further reduce the signal to 9.6 fb, because most of events are lost due to the  $p_T$  cut on the not-so-energetic  $\tau$ 's and the  $\Delta R(\tau^-, \tau^+)$  cut in each signal event. Considering the reconstruction efficiencies and the invariant mass cuts given in Eq. (42), the final reconstructed cross section is 0.33 fb.
2. When we fix  $m_\eta$  and increase  $m_h$ , we find that the final reconstructed cross section decreases. For instance when we take  $m_h = 155$  GeV, the reconstructed cross section is only 0.04 fb. This reduction is not only due to the decrease of the cross section  $\sigma(pp \rightarrow h\eta)$  but also due to the onset of the mode  $h \rightarrow WW^*$ .
3. Unlike MSSM and NMSSM, there is no dramatic enhancement due to large  $t_\beta$  for the  $pp \rightarrow h\eta \rightarrow b\bar{b}\tau^+\tau^-$  than the chosen benchmark point in Eq.(43). First the parameter  $t_\beta$  has an upper bound by the validity of perturbation expansion [7]. Second, the coupling of  $Z$ - $h$ - $\eta$  is around half of  $g_Z$ , which is almost the maximum value in the allowed parameter space. Third, the branching ratio of  $\text{Br}(\eta \rightarrow \tau^-\tau^+)$  cannot change

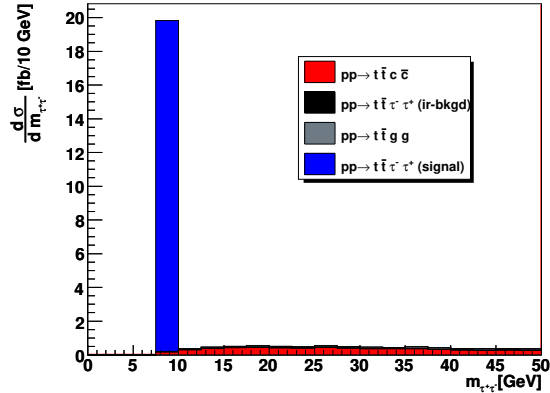


FIG. 9: The invariant mass distributions of  $m_{\tau\tau}$  for the signal and various backgrounds in  $pp \rightarrow t\bar{t}\eta \rightarrow t\bar{t}\tau^-\tau^+$  after imposing the selection cuts.

drastically with the increase of  $t_\beta$ . This is to be compared with the MSSM and NMSSM model cases where both the  $Z$ - $h$ - $\eta$  coupling and the branching ratio of  $\text{Br}(\eta \rightarrow \tau^-\tau^+)$  might be enhanced by factors of 1.5 and 1.5, respectively.

## VI. THE SIGNAL AND BACKGROUNDS OF $pp \rightarrow t\bar{t}\eta$

In this section we study the signal and backgrounds of  $pp \rightarrow t\bar{t}\eta$ , focused on the benchmark point in Eq. (43). For simplicity we first assume that the reconstruction efficiency of the top quark is 100 percent and can be fully reconstructed. We can focus on the analysis of the signal and the most direct backgrounds at the  $t$  and  $\bar{t}$  level. The majority of backgrounds comes from  $t\bar{t}jj$  with  $jj = c\bar{c}, gg, q\bar{q}$ , among which  $t\bar{t}c\bar{c}$  is the most serious background. This is because of poor rejection factor of the charm quark, which behaves similarly to a  $\tau$ -jet. Another source of background is  $t\bar{t}\tau^+\tau^-$ , which is irreducible but essentially small because the  $\tau$ 's are produced mostly off a virtual photon or a  $Z$  boson.

We note that the invariant mass cut on  $m_{\tau\tau}$  is very crucial for signal event selection. It removes most of irreducible backgrounds, in which the two  $\tau$ 's are emitted from a virtual photon,  $Z$ , or a Higgs boson. It also suppresses the  $t\bar{t}c\bar{c}$  background effectively. In Fig. 9, we show the spectrum of  $m_{\tau\tau}$  for both the signal and the major backgrounds. It is obvious that the signal clearly stands out of the backgrounds.

In Table II, we show the cross sections of major backgrounds and signal after cuts. Here

Background processes	Cross Section (fb)
$t\bar{t}c\bar{c}$	0.17
$t\bar{t}\tau^-\tau^+$	0.02
$t\bar{t}gg$	0.02
Signal processes	Cross Section (fb)
$t\bar{t}\tau^-\tau^+$	19.6

TABLE II: Cross sections for the signal and various backgrounds in  $pp \rightarrow t\bar{t}\tau^-\tau^+$  after imposing all cuts

we comment on the signal in more detail. The total cross section of the  $pp \rightarrow t\bar{t}\eta$  process is about 500 fb. After imposing the kinematic cuts on the  $\tau$ 's, the cross section is reduced to about 120 fb. Including the reconstruction efficiency of  $\tau$ 's, it further reduces to about 19 fb. Note that we have only analyzed down to the  $t$  and  $\bar{t}$  level. If we take the top-quark decays into account, there should be more backgrounds such as  $W^+W^- + \text{jets}$  and  $W^\pm + \text{jets}$ . However, these backgrounds are electroweak in nature and thus much smaller than the QCD production of  $t\bar{t}c\bar{c}$ .

The signal-to-background ratio seems quite promising. However, we still need to apply the top quark reconstruction and identification efficiencies. For a simple estimate of the top quark reconstruction, we should include the reconstruction efficiency of two  $b$  jets and two  $W$ 's. With one of the  $W$ 's decaying leptonically ( $e$  and  $\mu$ ) while the other one decaying hadronically, the reduction factor is therefore

$$f = e_b^2 \times 2 \times \frac{6}{9} \times \frac{2}{9}. \quad (44)$$

where  $e_b \approx 50\%$  is the  $B$ -tagging efficiency. Thus, the more realistic reconstructed cross section of  $pp \rightarrow t\bar{t}\tau^-\tau^+$  is estimated to be 1.5 fb. Even taking into account the selection cuts for the decay products of the top quark, we should still have enough signal events per LHC year.

## VII. CONCLUSIONS

We have performed a comprehensive study on the decays and production of the pseudoscalar boson  $\eta$  of the simplest little Higgs model at the LHC. We focus on the mass range of  $m_\eta < 2m_b$  such that the dominant decay mode is  $\eta \rightarrow \tau^+\tau^-$ , followed by  $gg$  and  $c\bar{c}$ . The decay branching ratio into  $\gamma\gamma$  is only of the order of  $10^{-4}$ .

The dominant production channel is gluon fusion ( $gg \rightarrow \eta$ ), followed by  $b\bar{b}$  fusion ( $b\bar{b} \rightarrow \eta$ ). However, the sole  $\eta \rightarrow \tau^+\tau^-$  in the final state may be buried under the Drell-Yan background in this invariant mass region. We have therefore focused on the associated production channels of  $pp \rightarrow h\eta$  and  $pp \rightarrow t\bar{t}\eta$ . We have shown that  $t\bar{t}\eta$  production is in fact large enough to give a sizable number of events while suppressing the backgrounds, the majority of which comes from  $t\bar{t}c\bar{c}$ . On the other hand,  $h\eta \rightarrow b\bar{b}\tau^+\tau^-$  suffers severely from the  $b\bar{b}c\bar{c}$  background. Unless experiments can achieve a very high rejection factor for charm quark, this channel remains pessimistic.

### APPENDIX A: HELICITY AMPLITUDES FOR $q\bar{q} \rightarrow t\bar{t}\eta$ AND $gg \rightarrow t\bar{t}\eta$

For the process of

$$q(k_1, i) + \bar{q}(k_2, j) \rightarrow t(p_1, l) + \bar{t}(p_2, m) + \eta(p_3),$$

there are two contributing Feynman diagrams, as shown in Fig. 10. Here the 4-momenta and the color indices  $(i, j, l, m)$  are given in parenthesis. The amplitudes are

$$\begin{aligned} iM_1 &= \frac{ig_{\eta tt}g_s^2T_{ji}^aT_{lm}^a}{(k_1+k_2)^2((p_1+p_3)^2-m_t^2)} \bar{u}(p_1)\gamma^5 \not{p}_3\gamma^\mu v(p_2) \bar{v}(k_2)\gamma_\mu u(k_1), \\ iM_2 &= -\frac{ig_{\eta tt}g_s^2T_{ji}^aT_{lm}^a}{(k_1+k_2)^2((p_2+p_3)^2-m_t^2)} \bar{u}(p_1)\gamma^\mu \not{p}_3\gamma^5 v(p_2) \bar{v}(k_2)\gamma_\mu u(k_1), \end{aligned}$$

where  $g_{\eta tt} = \sqrt{2} \cot 2\beta(m_t/f)$  and the interaction Lagrangian is  $\mathcal{L} = -ig_{\eta tt}\eta \bar{f}\gamma^5 f$ .

There are eight Feynman diagrams, as depicted in Fig. 10, contributing to the subprocess

$$g(k_1, a) + g(k_2, b) \rightarrow t(p_1, j) + \bar{t}(p_2, i) + \eta(p_3)$$

where  $a, b, i, j$  are color indices. The  $t$ -channel-like helicity amplitudes are

$$\begin{aligned}
iM_A &= \frac{iA}{(2p_1 \cdot p_3 + m_\eta^2)(2k_2 \cdot p_2)} \bar{u}(p_1) \gamma^5 \not{p}_3 \gamma^\mu (\not{k}_2 - \not{p}_2 + m_t) \gamma^\nu v(p_2) \epsilon_\mu(k_1) \epsilon_\nu(k_2), \\
iM_B &= \frac{-iA}{4(k_1 \cdot p_1)(k_2 \cdot p_2)} \bar{u}(p_1) \gamma^5 \gamma^\mu (\not{p}_1 - \not{k}_1 - m_t) (\not{k}_2 - \not{p}_2 + m_t) \gamma^\nu v(p_2) \epsilon_\mu(k_1) \epsilon_\nu(k_2), \\
iM_C &= \frac{-iA}{(2p_2 \cdot p_3 + m_\eta^2)(2k_1 \cdot p_1)} \bar{u}(p_1) \gamma^5 \gamma^\mu (\not{p}_1 - \not{k}_1 - m_t) \gamma^\nu \not{p}_3 v(p_2) \epsilon_\mu(k_1) \epsilon_\nu(k_2). \quad (\text{A1})
\end{aligned}$$

The  $u$ -channel-like ones are

$$\begin{aligned}
iM_D &= \frac{-iB}{(2p_2 \cdot p_3 + m_\eta^2)(2k_2 \cdot p_1)} \bar{u}(p_1) \gamma^5 \gamma^\nu (\not{p}_1 - \not{k}_2 - m_t) \gamma^\mu \not{p}_3 v(p_2) \epsilon_\mu(k_1) \epsilon_\nu(k_2), \\
iM_E &= \frac{-iB}{4(k_1 \cdot p_2)(k_2 \cdot p_1)} \bar{u}(p_1) \gamma^5 \gamma^\nu (\not{p}_1 - \not{k}_2 - m_t) (\not{k}_1 - \not{p}_2 + m_t) \gamma^\mu v(p_2) \epsilon_\mu(k_1) \epsilon_\nu(k_2), \\
iM_F &= \frac{iB}{(2p_1 \cdot p_3 + m_\eta^2)(2k_1 \cdot p_2)} \bar{u}(p_1) \gamma^5 \not{p}_3 \gamma^\nu (\not{k}_1 - \not{p}_2 + m_t) \gamma^\mu v(p_2) \epsilon_\mu(k_1) \epsilon_\nu(k_2). \quad (\text{A2})
\end{aligned}$$

The  $s$ -channel-line ones are

$$\begin{aligned}
iM_G &= \frac{E}{(2p_1 \cdot p_3 + m_\eta^2)(2k_1 \cdot k_2)} \bar{u}(p_1) \gamma^5 \not{p}_3 ((\not{k}_1 - \not{k}_2) g^{\mu\nu} + 2k_2^\mu \gamma^\nu - 2k_1^\nu \gamma^\mu) v(p_2) \epsilon_\mu(k_1) \epsilon_\nu(k_2), \\
iM_H &= \frac{-E}{(2p_2 \cdot p_3 + m_\eta^2)(2k_1 \cdot k_2)} \bar{u}(p_1) \gamma^5 ((\not{k}_1 - \not{k}_2) g^{\mu\nu} + 2k_2^\mu \gamma^\nu - 2k_1^\nu \gamma^\mu) \not{p}_3 v(p_2) \epsilon_\mu(k_1) \epsilon_\nu(k_2),
\end{aligned}$$

where the constant factors  $A, B, E$  are given by

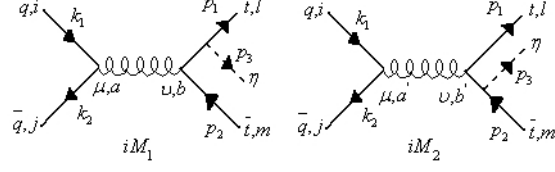
$$A \equiv g_{\eta tt} g_s^2 (T^a T^b)_{jl}, \quad B \equiv g_{\eta tt} g_s^2 (T^b T^a)_{jl}, \quad E \equiv g_{\eta tt} g_s^2 f^{abc} T_{jl}^c.$$

## APPENDIX B: DECAY OF $Z'$

The heavy gauge boson  $Z'$  decays into the SM fermions ( $Z' \rightarrow f\bar{f}$ ) and into the Higgs and  $\eta$  bosons ( $Z' \rightarrow \eta H$ ). We neglect the decay of  $Z' \rightarrow W^+ W^-$  since the vertex is suppressed by  $v^2/f^2$ , without  $t_\beta$  enhancement. In spite of non-suppressed  $Z'$ - $X^+$ - $X^-$  and  $Z'$ - $Y^0$ - $\bar{Y}^0$  couplings, the mass relation of  $M_{X,Y} \approx 0.82 M_{Z'}$  does not allow the decay of  $Z' \rightarrow X^+ X^-, Y^0 \bar{Y}^0$ . Decay rates are

$$\begin{aligned}
\Gamma(Z' \rightarrow f\bar{f}) &= \frac{N_C}{24\pi} g_Z^2 \left[ (g_{2R}^f)^2 + (g_{2L}^f)^2 \right] M_{Z'}, \quad (\text{B1}) \\
\Gamma(Z' \rightarrow \eta H) &= \frac{c_2^2}{192\pi} \lambda^{3/2} M_{Z'},
\end{aligned}$$

$$q(k_1) + \bar{q}(k_2) \rightarrow t(p_1) + \bar{t}(p_2) + \eta(p_3)$$



$$g(k_1) + g(k_2) \rightarrow t(p_1) + \bar{t}(p_2) + \eta(p_3)$$

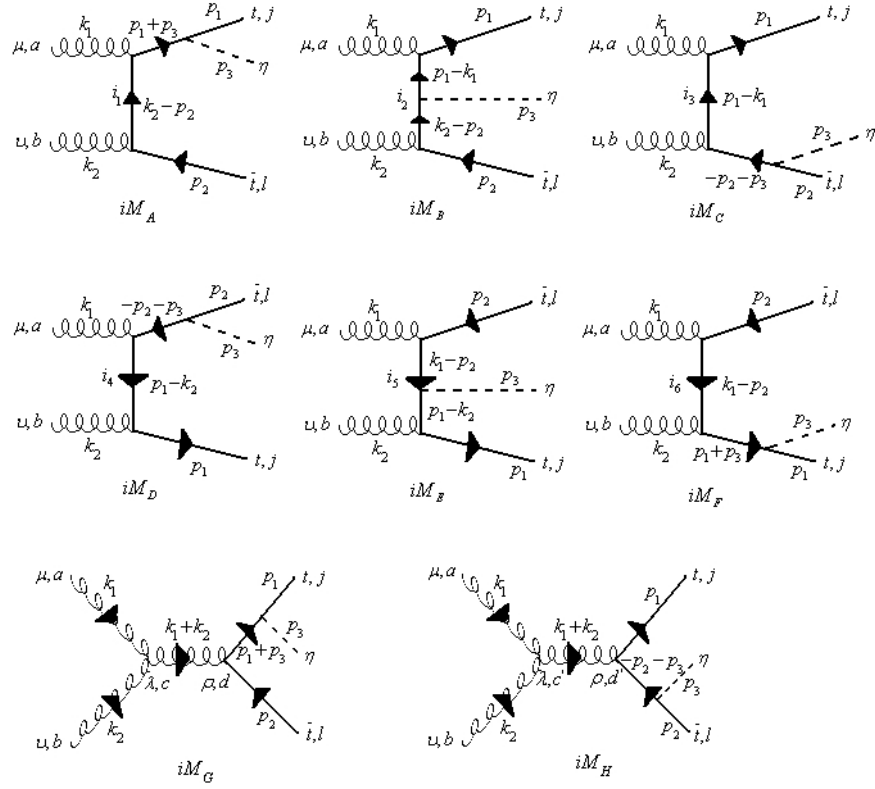


FIG. 10: Feynman diagrams for  $q\bar{q} \rightarrow t\bar{t}\eta$  and  $gg \rightarrow t\bar{t}\eta$

where  $\lambda = 1 + (m_\eta/M_{Z'})^4 + (m_H/M_{Z'})^4 - 2(m_\eta/M_{Z'})^2 - 2(m_H/M_{Z'})^2 - 2(m_\eta/M_{Z'})^2(m_H/M_{Z'})^2$ . We refer the expression of  $c_2$  and  $g_{2R,2L}^f$ 's for  $f = u, d, c, s, b$  to Eq. (29). Other couplings are

$$\begin{aligned} g_{2R}^t &= \frac{2}{3} \frac{x_W}{\sqrt{3-4x_W}}, & g_{2L}^t &= \frac{1}{\sqrt{3-4x_W}} \left( \frac{1}{2} - \frac{1}{3}x_W \right), \\ g_{2R}^e &= -\frac{x_W}{\sqrt{3-4x_W}}, & g_{2L}^e &= \frac{1}{\sqrt{3-4x_W}} \left( \frac{1}{2} - x_W \right), \\ g_{2R}^\nu &= 0, & g_{2L}^\nu &= \frac{1}{\sqrt{3-4x_W}} \left( \frac{1}{2} - x_W \right), \end{aligned} \quad (\text{B2})$$

## ACKNOWLEDGMENTS

The work of JS is supported by the Korea Research Foundation Grant (KRF-2005-070-c00030). The work of KC, PT, and QSY is supported by the NSC under grant no. NSC 96-2628-M-007-002-MY3 and the NCTS.

- 
- [1] R. Barate *et al.* [LEP Working Group for Higgs boson searches], Phys. Lett. B **565**, 61 (2003).  
[2] The LEP Electroweak Working Group, the latest result is in <http://lepewwg.web.cern.ch/LEPEWWG/>  
[3] N. Arkani-Hamed, A. G. Cohen and H. Georgi, Phys. Lett. B **513**, 232 (2001); N. Arkani-Hamed, A. G. Cohen, E. Katz, A. E. Nelson, T. Gregoire and J. G. Wacker, JHEP **0208**, 021 (2002); N. Arkani-Hamed, A. G. Cohen and H. Georgi, Phys. Lett. B **513**, 232 (2001); M. Perelstein, arXiv:hep-ph/0512128.  
[4] N. Arkani-Hamed, A. G. Cohen, E. Katz and A. E. Nelson, JHEP **0207**, 034 (2002);  
[5] M. Schmaltz, JHEP **0408**, 056 (2004).  
[6] J. A. Casas, J. R. Espinosa and I. Hidalgo, JHEP **0503**, 038 (2005).  
[7] K. Cheung and J. Song, Phys. Rev. D **76**, 035007 (2007) [arXiv:hep-ph/0611294].  
[8] D. E. Kaplan and M. Schmaltz, JHEP **0310**, 039 (2003).  
[9] W. Kilian, D. Rainwater and J. Reuter, Phys. Rev. D **71**, 015008 (2005).  
[10] N. Brambilla *et al.* [Quarkonium Working Group], arXiv:hep-ph/0412158; W. M. Yao *et al.* [Particle Data Group], J. Phys. G **33** (2006) 1; R. Balest *et al.* [CLEO Collaboration], Phys. Rev. D **51**, 2053 (1995).  
[11] K. Cheung, J. Song and Q. S. Yan, Phys. Rev. Lett. **99**, 031801 (2007) [arXiv:hep-ph/0703149].

- [12] T. Han, H. E. Logan and L. T. Wang, JHEP **0601**, 099 (2006).
- [13] O. C. W. Kong, arXiv:hep-ph/0307250; O. C. W. Kong, J. Korean Phys. Soc. **45**, S404 (2004).
- [14] K. Cheung, C. S. Kim, K. Y. Lee and J. Song, arXiv:hep-ph/0608259.
- [15] G. Bagliesi *et al.*, “Tau jet reconstruction and tagging at high level trigger and off-line,” CERN-CMS-NOTE-2006-028, Jan 2006.